Damage detection in multi-span beams based on the analysis of frequency changes

G R Gillich[1], J L Ntakpe[1,2], M Abdel Wahab[3], Z I Praisach[1] and M C Mimis[1]

[1]NDT Laboratory, Faculty of Engineering and Management, "Eftimie Murgu"
University of Resita, Romania
[2]Alphabet International GmbH, Munich, Germany
[3]Laboratory Soete, Faculty of Engineering and Architecture, Ghent University,
Belgium

E-mail: gr.gillich@uem.ro

Abstract. Crack identification in multi-span beams is performed to determine whether the structure is healthy or not. Among all crack identification methods, these based on measured natural frequency changes present the advantage of simplicity and easy to use in practical engineering. To accurately identify the cracks characteristics for multi-span beam structure, a mathematical model is established, which can predict frequency changes for any boundary conditions, the intermediate supports being hinges. This relation is based on the modal strain energy concept. Since frequency changes are relative small, to obtain natural frequencies with high resolution, a signal processing algorithm based on superposing of numerous spectra is also proposed, which overcomes the disadvantage of Fast Fourier Transform in the aspect of frequency resolution. Based on above-mentioned mathematical model and signal processing algorithm, the method of identifying cracks on multi-span beams is presented. To verify the accuracy of this identification method, experimental examples are conducted on a two-span structure. The results demonstrate that the method proposed in this paper can accurately identify the crack position and depth.

1. Introduction

Even if beams with multiple supports are frequently used in practice, the research about such structures in the damaged state is not broadly present in the literature. In this research, uniformly spaced spans are commonly considered. An example is the study of a beam with two identical spans traversed by a train moving at a constant velocity, which had the aim to highlight the resonance characteristics [1]. The Euler-Bernoulli beam theory was used to model the two beam segments, and constraints and compatibility conditions were imposed at the beam center. The effect of the random deviation of the span lengths from the ideal design was studied in [2], using the perturbation method. Transverse vibrations of a slender beam with infinite length mounted on discrete elastic supports are studied in [3]. To describe the dynamic behavior of multi-span beams, the supports are replaced by forces acting on the support locations. The deflection is described by a single function, the reactions at the support locations being included in the eigenvalue solution [4].

In the damage detection methods, the multi-span structures with transverse cracks are treated as an assembly of intact sub-segments. The cracks are replaced with massless rotational spring, while instead of the supports, constraints and compatibility conditions are imposed [5]. The models become

complicated, and, by replacing the intermediate supports or the crack, a new set of equations has to be solved. Several theoretical studies and experiments aiming to study and analyze the changes of the natural frequencies and mode shapes occurring due to damage in general terms [6-13] and due to a crack in particular [14-17], were presented in the literature.

Previous publications, [18-20], present a mathematical relation that predicts the frequency changes occurred in single span beams due to cracks with known depth and position. The input data is limited to the curvature achieved by the intact beam in the location where damage is expected, and the absolute damage severity derived from the deflections of the intact and damaged beam. Based on this relation a database was build for a multitude of damage scenarios and differently supported beams, therefore damage assessment becomes an inverse problem.

This paper presents the exact solution for the frequencies of beams with two unequal spans, for both healthy and damaged state. Any support and crack position can be taken into consideration; the crack depth is limited to around 50% by the linearity condition. The results are implemented in a database and used to demonstrate the robustness of the proposed damage assessment method.

2. Modal parameters for the intact two-span beam

The study is performed on a long slender beam with two spans, as shown in figure 1, having the length L, the width b and the thickness h, and consequently the second moment of area of the cross section I and the cross section area A. At the right end the support is a hinge and the left end is clamped; supplementary, a hinge at distance L_1 is intercalated. The relevant material characteristics are: the Young Modulus E, the volumetric mass density ρ, and the Poisson ratio μ.

If the beam is subjected to a damage, this is an open transversal crack which has the depth a and the width l. Its position is indicated as c.
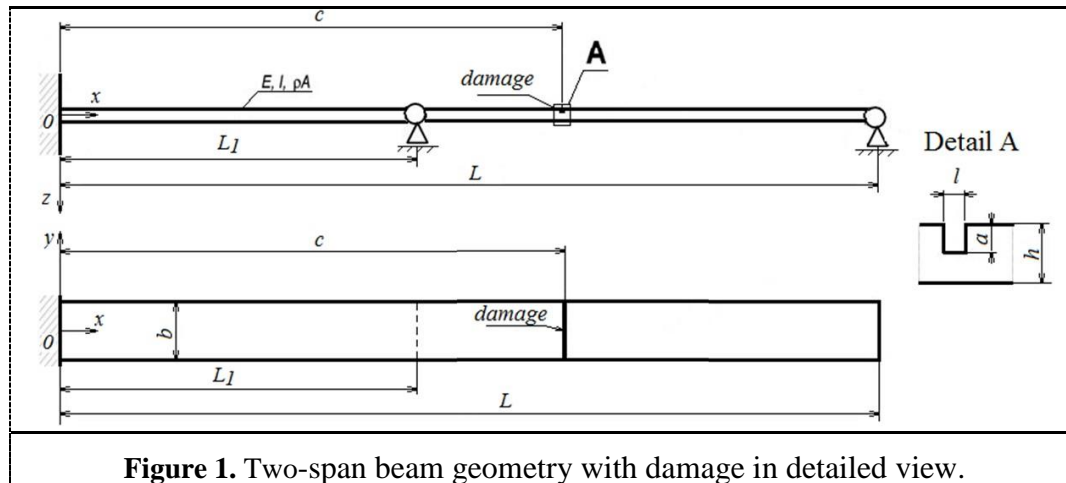

Figure 1. Two-span beam geometry with damage in detailed view.

The bending vibrations of this beam are described by the following equation:

$$\frac{\partial^4 z}{\partial x^4} + \frac{\rho A}{EI} \cdot \frac{\partial^2 z}{\partial t^2} = 0 \tag{1}$$

where z is the vertical beam displacement at distance x measured from the left end. The solution z of equation (1) can be written as a standing wave, $z(x,t) = W(x) \cdot \sin(\omega t + \varphi)$, thus spatial and temporal components are separated. For the spatial component the well-known solution is

$$W(x) = A\sin\alpha x + B\cos\alpha x + C\sinh\alpha x + D\cosh\alpha x \tag{2}$$

where *A, B, C* and *D* and $\alpha^4 = \dfrac{\rho A \omega^2}{EI}$ are coefficients defined by the particular boundary conditions.
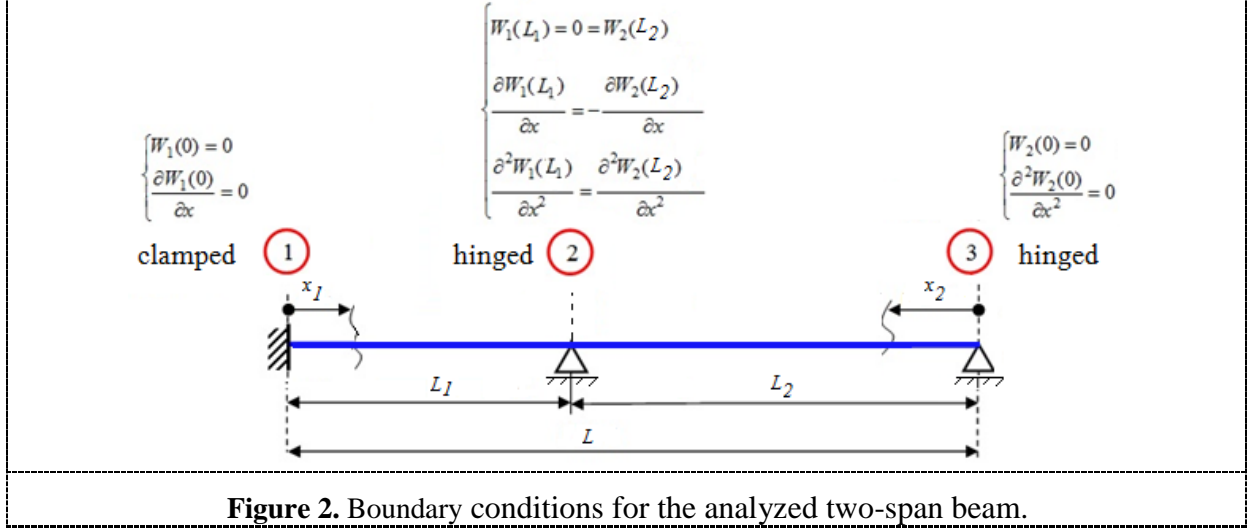

Figure 2. Boundary conditions for the analyzed two-span beam.

In the vibration analysis, each segment between two supports is considered as a separate beam. The left segment has associated the space interval $x_1 \in (0 \dots L_1)$, and the origin of the reference system is the fixed beam end (point 1 in figure 2). The right segment has associated the space interval $x_2 \in (0 \dots L_2)$, and the origin of the reference system is the hinge placed at the right beam end (point 3 in figure 2). The two solutions of equation (1) get, for the two segments, the form

$$\begin{cases} W_1(x_1) = A_1 \sin(\alpha x_1) + B_1 \cos(\alpha x_1) + C_1 \sinh(\alpha x_1) + D_1 \cosh(\alpha x_1) \\ W_2(x_2) = A_2 \sin(\alpha x_2) + B_2 \cos(\alpha x_2) + C_2 \sinh(\alpha x_2) + D_2 \cosh(\alpha x_2) \end{cases} \quad (3)$$

Applying the eight constraints and continuity conditions to the solutions in equation (3), it results a system with eight algebraic equations. After removing the eight coefficients $A_1 \dots D_2$ from the algebraic system, an equation with the variable $\lambda = \alpha / L$ is attained, that is
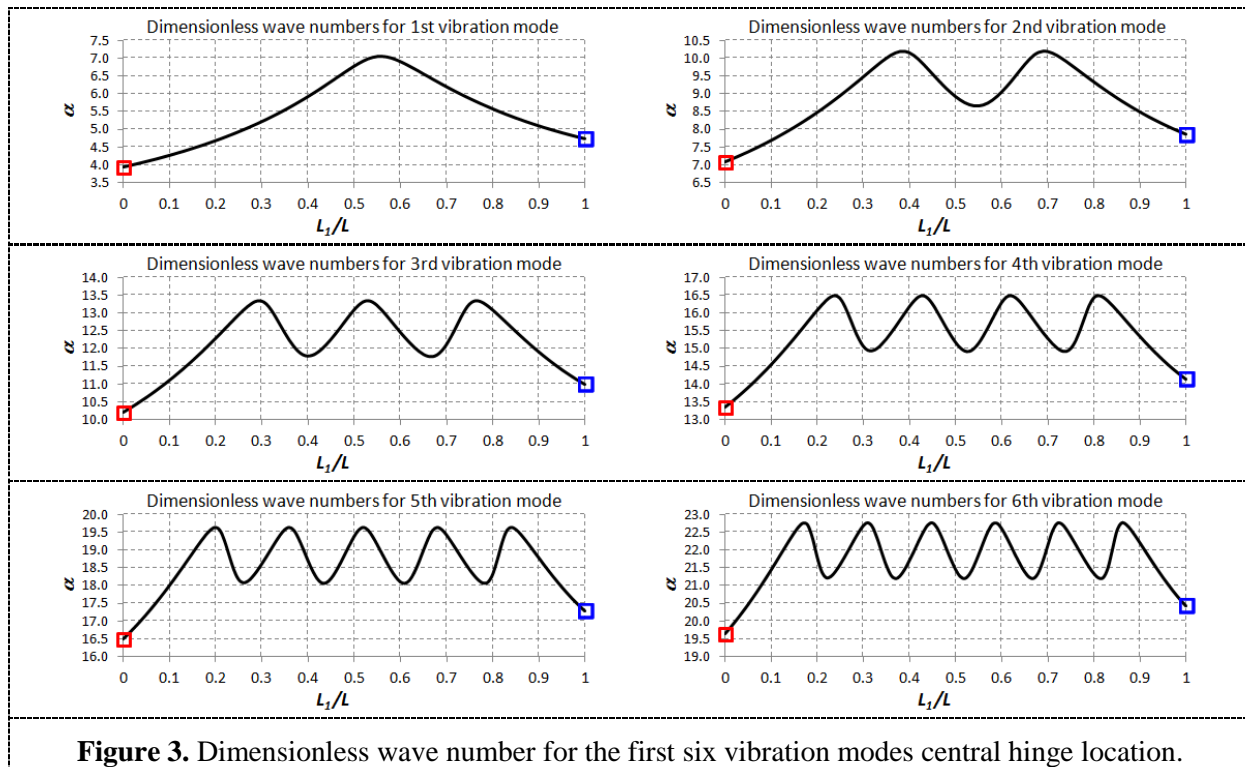
$$\begin{aligned} & 2 \cdot \left[\left(\Omega_1(\lambda L_1) \right)^2 + \Pi_1(\lambda L_1) \cdot \Gamma_1(\lambda L_1) \right] - \\ & - \left[\frac{\Sigma_1(\lambda L_1)\Pi_1(\lambda L_1) - \Omega_1(\lambda L_1)\Gamma_1(\lambda L_1)}{\sin(\lambda L_2)} \right] \cdot \left[\frac{\cos(\lambda L_2)}{\sin(\lambda L_2)} - \frac{\cosh(\lambda L_2)}{\sinh(\lambda L_2)} \right] = 0 \end{aligned} \quad (4)$$

where $\Gamma_1(\lambda L_1) = \sin(\lambda L_1) + \sinh(\lambda L_1)$, $\Pi_1(\lambda L_1) = \sin(\lambda L_1) - \sinh(\lambda L_1)$, $\Sigma_1(\lambda L_1) = \cos(\lambda L_1) + \cosh(\lambda L_1)$ and $\Omega_1(\lambda L_1) = \cos(\lambda L_1) - \cosh(\lambda L_1)$.

By solving equation (4) for the central hinge position removed iteratively along the beam, the evolution of the dimensionless wave number λ in form of variation curves is obtained (see figure 3). From this figure one can easily observe that for $\overline{L}_1 \to 0$ the wave numbers achieve very close values to that of a beam clamped at the left end and hinged at the right end (marked with a red square). If the intermediate hinge is close to the hinged end, i.e. $\overline{L}_1 \to 1$, the wave number values are very similar with that of a beam with both ends clamped (marked with a blue square).

The two-span beam's frequencies can be derived using the well-known frequency relation

$$f_i = \frac{\lambda_i^2}{2\pi} \sqrt{\frac{EI}{\rho A L^4}} \quad (5)$$

Figure 3. Dimensionless wave number for the first six vibration modes central hinge location.

By replacing the coefficients A_1, B_1, C_1, D_1, A_2, B_2, C_2, D_2 in equations (4), results the mode shape function for the considered continuous beam. For the left segment it is:

$$W_{1-i}\left(x_1, L_1, \lambda_i\right) = D_1\left\{\frac{\Omega_1\left(\lambda_i L_1\right)}{\Pi_1\left(\lambda_i L_1\right)}\cdot\left[\sin\left(\lambda_i x_1\right)-\sinh\left(\lambda_i x_1\right)\right]-\left[\cos\left(\lambda_i x_1\right)-\cosh\left(\lambda_i x_1\right)\right]\right\} \qquad (6)$$

while for the right segment it is:

$$W_{2-i}\left(x_2, L_1, \lambda_i\right) = D_1\frac{\Sigma_1(\lambda L_1)\Pi_1(\lambda L_1)-\Omega_1(\lambda L_1)\Gamma_1(\lambda L_1)}{2\cdot\Pi_1(\lambda L_1)\cdot\sin(\lambda L_2)}\left[\frac{\sin(\lambda_i L_2)}{\sinh(\lambda_i L_2)}\cdot\sinh\left(\lambda_i x_2\right)-\sin\left(\lambda_i x_2\right)\right] \quad (7)$$

Note that, to obtain normalized mode shapes, D_1 must be determined separately for each location of L_1 and vibration mode.
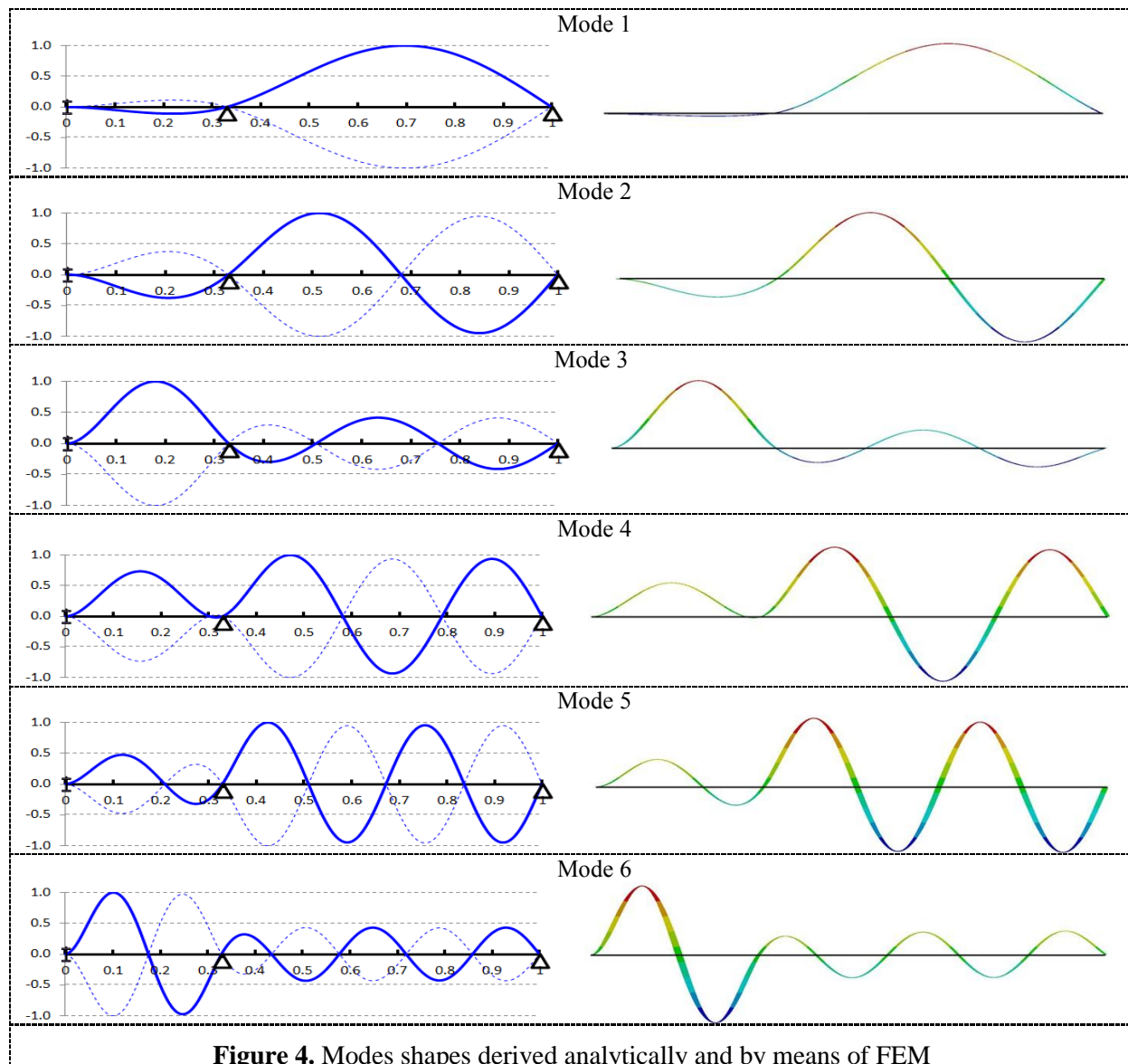
The analytically achieved results are now compared with that from FEM simulations. A beam with following geometrical and physical-mechanical parameters is involved in the analysis: $L = 2\,\text{m}$, $b = 20\,\text{mm}$, $h = 5\,\text{mm}$, $\rho = 7850\,\text{kg/m}^3$, $E = 2\cdot10^{11}\,\text{N/m}^2$ and $\nu = 0.3$. In the first case the central hinge is placed at the normalized distance $L_1 / L = 0.33$ and in the second case it is located at distance $L_1 / L = 0.45$. The FEM analysis, performed by means of the ANSYS 14 software, made use of a hexahedral mesh element with imposed dimensions 2 mm.

Table 1 indicates the wave numbers and frequencies derived analytically, as well as the simulation results. The differences between synonym frequencies is less than 5%, except two modes of the beam with central hinge at $L_1 / L = 0.33$. These differences occur because certain slenderness is necessary to permit applying the Euler-Bernoulli theory. Thus, if one of the beam segments is short, bigger errors are present, imposing a more complex model. In addition, the FEM model does not exactly reflect the conditions induced by the hinges in the analytical model.

Table 1. Wave numbers and frequencies for two position of the intermediate hinge.

| Vibration mode i | Hinge at $L_1/L = 0.33$ | | | Hinge at $L_1/L = 0.45$ | | |
| | Analytic | | FEM | Analytic | | FEM |
	Wave number	Frequency [Hz]	Frequency [Hz]	Wave number	Frequency [Hz]	Frequency [Hz]
1	5.407	8.475	9.358	6.348	11.681	12.538
2	9.806	27.873	27.334	9.569	26.542	27.789
3	12.908	48.296	53.050	12.264	43.593	43.824
4	15.008	65.292	65.813	16.262	76.662	81.506
5	19.219	107.073	106.538	18.196	95.978	99.190
6	22.358	144.903	150.784	22.773	150.341	151.798

For the hinge located at $L_1/L = 0.33$, the first six bending mode shapes are depicted in figure 4, where those corresponding to the analytic approach are to the left and those resulted from the FEM analysis to the right. One can observe in this figure that curves fit well.

Figure 4. Modes shapes derived analytically and by means of FEM

3. Natural frequencies of the damaged beam

The crack considered in this study is transversal and has the depth a, as shown in figure 1. It is located at distance c from the fixed end. As shown in our previous papers, the energy stored in a slice in the undamaged state can indicate the natural frequency drop if a crack occurs in that slice [19]. The mathematical relation permitting to determine the natural frequencies for the damaged beam, adapted for the particular case of the two-span beam is

$$f_{D-i}\left(c, L_1, \bar{a}\right) = f_i \left\{ 1 - \gamma(\bar{a}) \cdot \left[\bar{W}_i''\left(c, L_1, \alpha_i\right) \right]^2 \right\} \qquad (8)$$

where f_i is the natural frequency for the undamaged beam for the i-th vibration mode and $\gamma(\bar{a}) < 1$ is the damage severity characterizing the effect of a crack with relative depth [20], which is null for the undamaged beam. The normalized modal curvature at location c, denoted $\bar{W}_i''(c, L_1, \alpha_i)$ in equation (8), is found from equations (9) or (10), depending on which segment the crack is located.

$$W_{1-i}''\left(x_1, L_1, \alpha_i\right) = k_1 k_2 \left\{ -\frac{\Omega_1\left(\alpha_i L_1\right)}{\Pi_1\left(\alpha_i L_1\right)} \cdot \left[\sin\left(\alpha_i x_1\right) + \sinh\left(\alpha_i x_1\right) \right] + \left[\cos\left(\alpha_i x_1\right) + \cosh\left(\alpha_i x_1\right) \right] \right\} \quad (9)$$

$$W_{2-i}''\left(x_2, L_1, \alpha_i\right) = k_1 \frac{\Sigma_1(\alpha L_1)\Pi_1(\alpha L_1) - \Omega_1(\alpha L_1)\Gamma_1(\alpha L_1)}{2 \cdot \Pi_1(\alpha L_1) \cdot \sin(\alpha L_2)} \left[\frac{\sin(\alpha_i L_2)}{\sinh(\alpha_i L_2)} \cdot \sinh\left(\alpha_i x_2\right) - \sin\left(\alpha_i x_2\right) \right] \quad (10)$$

The functions in equations (9) and (10) are proportional with the modal curvatures of the two segments. Normalization is achieved by involving the proper coefficients k_1 and k_2. Based on equation (8), the frequencies of the damaged beam for any crack location can be calculated. Figure 5 shows the frequency evolution if the crack is replaced along the beam, for the intermediate hinge located at $L_1 / L = 0.33$. The damage severity is $\gamma(\bar{a}) = 0.01$; this severity is achieved for the open crack with depth $a = 1.25 \text{mm}$ and width $l = 2 \text{mm}$.
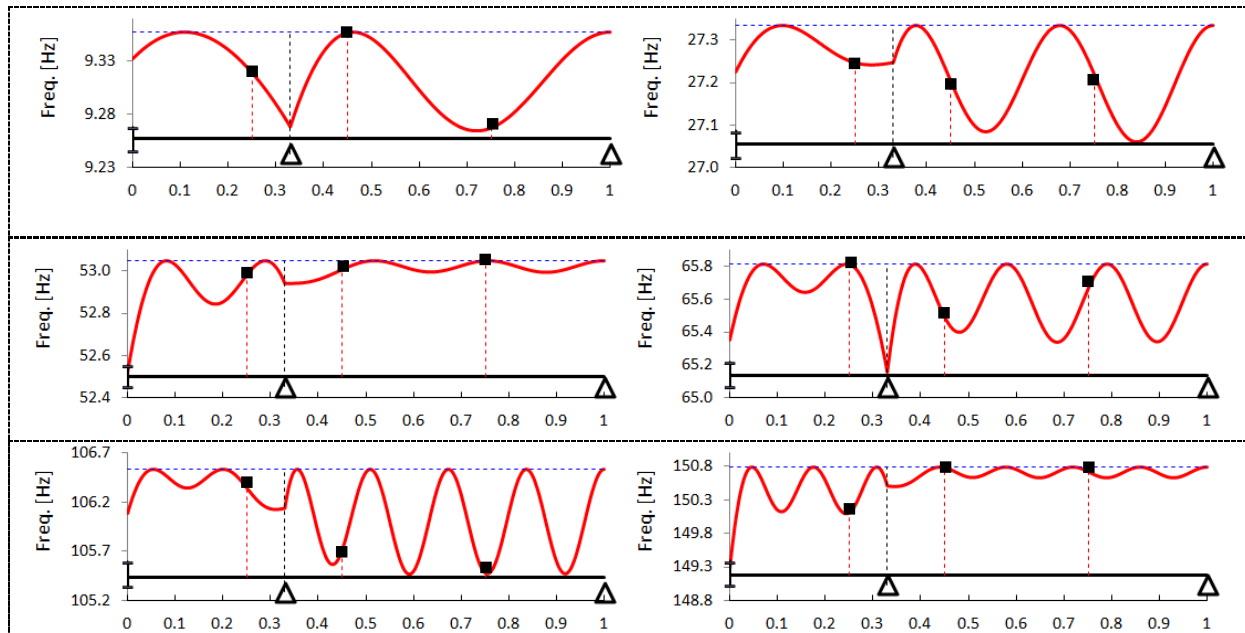

Figure 5. The frequency shift curves for the first six vibration modes analytically derived (red line) and samples attained from the FEM analysis.

Modal analysis using ANSYS was made for three crack positions $c_1/L = 0.25$, $c_2/L = 0.45$ and $c_3/L = 0.75$. The results are indicated with black squares in figure 5. Having a look onto this figure, it is easy to remark the fit between analytically and FEM-based attained results, meaning that equation (8) can be used to define damage patterns which can be further used in the damage detection process. For beams with multiple supports the frequency shifts are slight, making the improvement of frequency readability an important issue in experimental modal analysis [21-22].

4. The damage detection algorithm

The proposed assessment algorithm is based on the particularity that any crack provides a particular behavior change to that beam. As consequence of a crack, frequencies of different bending modes shift differently, in respect to the energy stored in the damaged slice, as shown in previous section. For the i-th bending mode of a two-span beam, the relative frequency shift is derived as:

$$\Delta \bar{f}_i(c, L_1, \bar{a}) = \frac{f_i - f_{D-i}}{f_i} = \gamma(\bar{a}) \cdot \left[\bar{W}_i''(c, L_1, \alpha_i) \right]^2 \tag{11}$$

For every damage locations c and relative depths $\bar{a}$ result the relative frequency shifts $\Delta \bar{f}_1 ... \Delta \bar{f}_n$ which constitute the damage pattern. In optimal conditions two frequency shifts are sufficient to identify location and severity [23], but an increased number of analyzed frequencies, we recommend $n > 6$, permit precise assessment because redundancy reduce evaluation or measurement errors.

Normalization of relative frequency shift values for each location c by the highest value of the sequence cancel the influence of damage depth. This happens because both numerator and denominator contain the severity $\gamma(\bar{a})$. In that way the sequence had become independent of the damage severity and its parameters take values between 0 and 1. Such a sequence is named Damage Location Indicator (DLI) and the individual parameters Damage Location Coefficients (DLC). For the crack positioned at distance c_j, the DLCs are

$$\Phi_1(c_j) = \frac{\left(\bar{W}_1''(c_j) \right)^2}{\max \left\{ \left(\bar{W}_i''(c_j) \right)^2 \right\}}, \quad ... , \Phi_n(c_j) = \frac{\left(\bar{W}_n''(c_j) \right)^2}{\max \left\{ \left(\bar{W}_i''(c_j) \right)^2 \right\}} \tag{12}$$
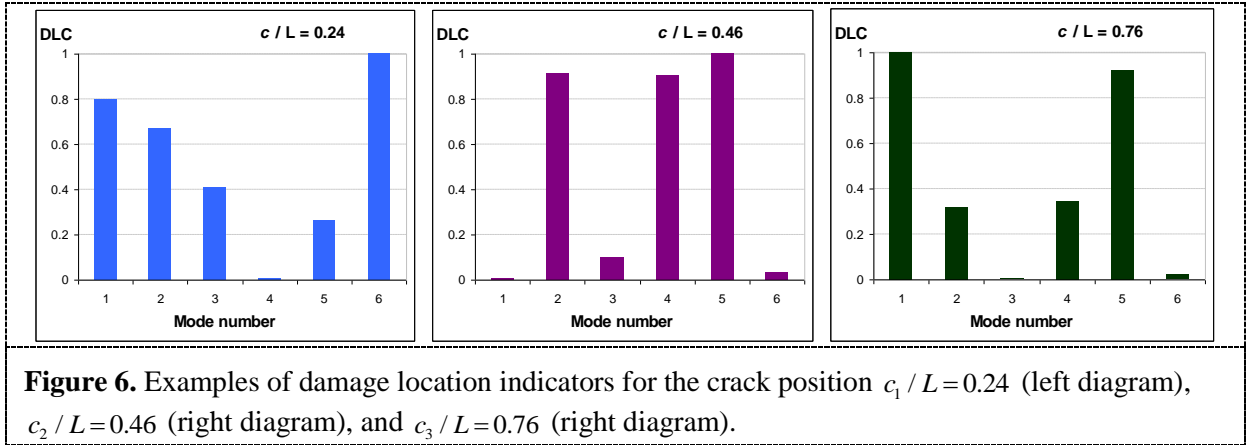
These DLCs can be derived just using information about the beam in its intact state. For asymmetric structures the DLCs uniquely indicate the damage location, while for symmetric structures two mirrored locations provide the same values of DLCs. An infinite number of damage location indicators, denoted $\Phi(c_j)$, can be derived in respect to the chosen crack positions j. From our expertise we recommend limiting to $p = 100$ locations.

For the real beam measured relative frequency shifts $\Delta \bar{f}_1^m ... \Delta \bar{f}_1^m$ can be also obtained from equation (11), if the frequencies in intact state f_i^m and in the presence of damage f_{D-i}^m are known. Normalizing the measured relative frequency shifts after the same rule as that used for the DLCs, the normalized measured frequency shifts NFR are obtained. These are expressed as

$$\Psi_1 = \frac{\Delta \bar{f}_1^m}{\max \left\{ \Delta \bar{f}_i^m \right\}}, \quad ... , \Psi_n = \frac{\Delta \bar{f}_n^m}{\max \left\{ \Delta \bar{f}_i^m \right\}} \tag{13}$$

and are also severity-independent. The entire sequence Ψ is nominated as the Damage Signature (DS); it has the same meaning as the DLIs but is derived from experimental data.

Example of two DLIs, for the beam with a hinge at $L_1/L = 0.33$ and damages at position $c_1/L = 0.24$, $c_2/L = 0.46$ and $c_3/L = 0.76$ are presented in figure 6.

Figure 6. Examples of damage location indicators for the crack position $c_1 / L = 0.24$ (left diagram), $c_2 / L = 0.46$ (right diagram), and $c_3 / L = 0.76$ (right diagram).

If the damage signature Ψ is compared with several damage location indicators $\Phi(c_j)$, it will be found one that best fit. The similitude test between the Damage Signature Ψ and all Damage Location Indicators $\Phi(c_j)$, in fact vectors with *n* elements, indicate the crack position by designating the index *j*. Herein the Minkowski distance of second order is uded as a Damage Index, that is

$$DI_j = \left(\sum_{i=1}^{n} \left| \Phi_i(c_j) - \Psi_i \right|^2 \right)^{\frac{1}{2}} \tag{14}$$

is used to find the most similar vectors. The value *j* for which the objective function DI*j* achieves the lowest value is searched; it indicates the crack location c_j .

Briefly, the proposed damage assessment algorithm is detailed in the following steps: If the beam is already damaged in the initial state, the assessment algorithm shows the damage evolution from this stage on.

S1 - frequency evaluation for the intact state is performed for the first *n* weak-axis bending vibration modes. It result a vector $U : \{ f_1^m ... f_n^m \}$

S2 - periodical measurements are performed, for each attempt being obtained a sequence $D : \{ f_{D-1}^m ... f_{D-n}^m \}$

S3 - frequencies for initial and actual state are compared in order to find the frequency shifts. The values obtained in step S2 are subtracted from those obtained in step S1, resulting $S : \{ \Delta f_1^m ... \Delta f_n^m \}$. For insignificant differences the structure is considered intact, else occurrence of damage is presumed.

S4 - if the damage is expected, the relative frequency shifts are determined as $R : \{ \Delta \bar{f}_1^m ... \Delta \bar{f}_n^m \}$

S5 - the relative frequency shifts are normalized, resulting the Damage Signature $\Psi : \{ \Psi_1 ... \Psi_n \}$

S6 - the normalized squared modal curvatures for the healthy beam are analytically determined for *p* equidistant locations, resulting *p* vectors $C_j : \left\{ \left[\bar{W}_{1,2-1}''(c_j, L_1, \bar{a}) \right]^2 ... \left[\bar{W}_{1,2-n}''(c_j, L_1, \bar{a}) \right]^2 \right\}$

S7 - the DLIs are derived by dividing the DLCs of each C_j to the highest value of the sequence, resulting $\Phi(c_j) : \left\{ \Phi_1(c_j) ... \Phi_n(c_j) \right\}$

S8 - the analytically derived $\Phi(c_j)$ vectors are compared to the Ψ vector determined by measurements by means of a similitude estimator (herein the Minkowski Distance) in order to identify the index *j* ensuring the lowest value, and subsequent the crack position c_j .

S9 - the damage severity can be determined from severity curves traced for different cross-sections after a methodology presented in [24].

5. Numerical experiment

The algorithm is tested for the three damages indicated at the end of section 3, with absolute positions $c_1 = 500$ mm, $c_2 = 900$ mm and $c_3 = 1500$ mm. The beam described in figure 1 is analyzed. It has the geometry and the physical-mechanical parameters provided in section 2, and the intermediate hinge position is at the position $L_1 = 660$ mm, resulting $L_1 / L = 0.33$.

The measurements are replaced by FEM simulations, the evaluated frequencies for the intact as well as for the three damage cases being presented in tables 2 to 4. We worked through steps the first 5 steps of the algorithm and found the RFS and the damage signatures Ψ for the three analyzed cases. These are compared in tables 2 to 4 with the DLCs of the closest damage location indicators. Note that, in steps S6 to S8, just 51 crack locations are considered. The reduced number of DLIs assumed in the database increases the degree of difficulty for the identification process. If crack identification is performed successful, it is demonstrated that the damage signature attained from six vibration modes doubtless indicate the crack position.

Table 2. Frequencies and damage patterns for the crack positioned at $c_1 = 500$ mm.

Vibration mode i	Intact	Damage at $c_1 = 500$ mm			Closest found DLCs	
	Frequency [Hz]	Frequency [Hz]	RSF	DS	DLC 480	DLC 520
1	9.358	9.316	0.4400	1	0.7987	1
2	27.334	27.245	0.3224	0.7327	0.6740	0.6947
3	53.050	52.991	0.1103	0.2508	0.4067	0.1623
4	65.813	65.800	0.0193	0.0439	0.0065	0.0562
5	106.538	106.326	0.1984	0.4509	0.2643	0.4919
6	150.784	150.160	0.4136	0.9400	1	0.8332

Table 3. Frequencies and damage patterns for the crack positioned at $c_2 = 900$ mm.

Vibration mode i	Intact	Damage at $c_2 = 900$ mm			Closest found DLCs	
	Frequency [Hz]	Frequency [Hz]	RSF	DLC	DLC 880	DLC 920
1	9.358	9.357	0.0080	0.0122	0.0309	0.0075
2	27.334	27.186	0.5402	0.8182	0.4323	0.9147
3	53.050	53.014	0.0661	0.1002	0.1134	0.0968
4	65.813	65.458	0.5379	0.8147	0.4504	0.9058
5	106.538	105.834	0.6601	1	1	1
6	150.784	150.758	0.0168	0.0255	0.0001	0.0319

Table 4. Frequencies and damage patterns for the crack positioned at $c_3 = 1500$ mm.

Vibration mode i	Intact	Damage at $c_3 = 1500$ mm			Closest found DLCs	
	Frequency [Hz]	Frequency [Hz]	RSF	DLC	DLC 1480	DLC 1520
1	9.358	9.266	0.9838	1	1	0.9681
2	27.334	27.236	0.3582	0.3721	0.3184	0.5139
3	53.050	53.048	0.0034	0.0033	0.0044	0.0001
4	65.813	65.616	0.2987	0.2962	0.3459	0.1447
5	106.538	105.544	0.9327	0.9521	0.9247	1
6	150.784	150.736	0.0312	0.0335	0.0215	0.0669

Similitude tests between the damage signatures and the damage location indicators are performed in step eight. The three vectors Ψ are individually compared with $p = 51$ vectors $\Phi(c_j)$ involving the Minkowski distance of second order. The results are graphically represented in figure 7, in the form of evolution curves. This figure gives direct information about the damage location. The similitude curve traced for the damage position $c_1 = 500$ mm attains the lowest values around the crack position, framing it. A clear minima is achieved for the crack positioned at $c_2 = 900$ mm, while the curve for the crack located at $c_3 = 1500$ mm present two possible solutions. A supplementary test can be performed by comparing the individual elements of the possible DLIs and the DS. Because the DS can fit just one DLI, this will indicate the damage position.
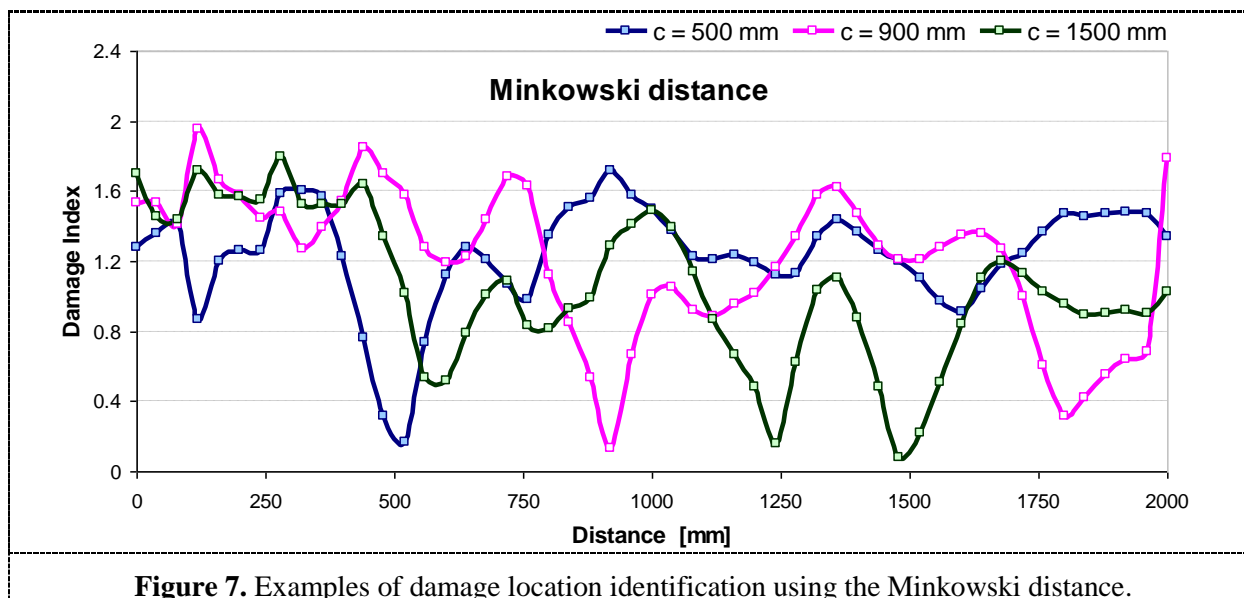

Figure 7. Examples of damage location identification using the Minkowski distance.

Alternatively, the damage position can be found by identifying the index *j* for which the damage index in equation (14) get the lowest value(s). This process can be automated, no human intervention being necessary. If more DI values qualify as possible solutions, in order to eliminate misinterpretation, again the individual elements of the potential DLIs and the DS can be compared.

In both analysis strategies, the increase of DLIs populating the database leads to an improved precision in locating cracks. This is reflected in damage index values close to null, eliminating doubts.

6. Conclusion

The problem of crack assessment in multi-span beams was considered via a simple and robust vibration-based method. The proposed method is based on the effect that the energy loss in a slice due to damage has upon the magnitude of frequency change. For the intact beam, the energy distribution in various vibration modes was contrived, and a predictive behavioral model developed. This model is used to define DLIs, which are integrated in a database including any possible damage scenarios for the analyzed beam. Adaption of the model, allowing the use of other end supports, can by simply made by changing the boundary conditions.

The method proved effective in detecting cracks and high accuracy is achieved in estimating the crack position. However, the early observation and precise localization depend on the possibility to quantify slight frequency changes and on the density of DLIs involved in the analysis. The similarity estimation strategy plays also a crucial role.

References

[1] Wang Y, Wei Q C, Shi J and Long X 2010 Resonance characteristics of two-span continuous beam under moving high speed trains *Latin American Journal of Solids and Structures* **7**(2) 185-199

[2] Yang J N and Lin Y K 1964Frequency Response Functions of a Disordered Periodic Beam *Journal of Sound and Vibration* **38**(3) 317–340.

[3] Hosking R J, Husain S A and Milinazzo F 2004 Natural flexural vibrations of a continuous beam on discrete elastic supports *Journal of Sound and Vibration* **272** 169–185.

[4] Khodabakhsh S and Bhat R B 2011 Clustered natural frequencies in multi-span beams with constrained characteristic functions *Shock and Vibration* **18** 698-707.

[5] Lien T V and Hao T A 2014 Determination of the Shape Function of a Multiple racked Beam Element and Its Application for the Free Vibration Analysis of a Multiple Cracked Frame Structure, *American Journal of Civil Engineering and Architecture* **2**(1) 12-15.

[6] Zhou Y-L, Maia NMM, Sampaio R and Wahab MA 2016 Structural damage detection using transmissibility together with hierarchical clustering analysis and similarity measure *Structural health monitoring* DOI: **https://doi.org/10.1177/1475921716680849**

[7] Zhou Y-L, Maia N and Abdel Wahab M 2016 Damage detection using transmissibility compressed by principal component analysis enhanced with distance measure *Journal of Vibration and Control* doi: 10.1177/1077546316674544

[8] Zhou Y-L and Abdel Wahab M 2016 Rapid early damage detection using transmissibility with distance measure analysis under unknown excitation in long-term health monitoring *Journal of Vibroengineering* **18**(7) 4491-4499

[9] Khatir S, Belaidi I, Serra R, Abdel Wahab M and Khatir T 2016 Numerical study for single and multiple damage detection and localization in beam-like structures using BAT algorithm *Journal of Vibroengineering* **18**(1) 202-213

[10] Khatir A, Tehami M, Khatir S and Abdel Wahab M 2016 Multiple damage detection and localization in beam‑like and complex structures using co-ordinate modal assurance criterion combined with firefly and genetic algorithms *Journal of Vibroengineering* **18**(8) 5063‑5073

[11] Gillich G-R, Praisach Z-I, Abdel Wahab M, Gillich N, Mituletu IC and Nitescu C 2016 Free vibration of a perfectly clamped-free beam with stepwise eccentric distributed masses *Shock and Vibration* **2016**(Article ID 2086274) 10 pages; http://dx.doi.org/10.1155/2016/2086274

[12] Khatir S, Belaidi I, Serra R, Abdel Wahab M and Khatir T 2015 Damage detection and localization in composite beam structures based on vibration analysis *Mechanika* **21**(6) 472-479

[13] Zhou Y-L and Abdel Wahab M 2017 Cosine based and extended transmissibility damage indicators for structural damage detection *Engineering Structures* **141** 175-183

[14] Li S G and Li H 2011 The Fractional Diagnosis of Multi-Span Continuous Bridge's Structural Damage Based on Neural Network and Genetic Algorithm *Applied Mechanics and Materials* **71-78** 1298-1304.

[15] Kullaa J, Santaoja K and Eymery A 2013 Vibration-based structural health monitoring of a simulated beam with a breathing crack *Key Engineering Materials* **569-570** 1093-1100.

[16] Surace C, Ruotolo R, Storer D 2011 Detecting nonlinear behaviour using the volterra series to assess damage in beam-like structures *Journal of Theoretical and Applied Mechanics* **49** 905-926.

[17] Sakellariou J S and Fassois S D 2008 Vibration based fault detection and identification in an

aircraft skeleton structure via a stochastic functional model based method *Mechanical Systems and Signal Processing* **22**(3) 557-573.

[18]   Gillich G R and Praisach Z I 2013 Detection and Quantitative Assessment of Damages in Beam Structures Using Frequency and Stiffness Changes *Key Eng. Mat.* **569-570** 1013-1020.

[19]   Gillich G R, Praisach Z I and Negru I 2012 Damages Influence on Dynamic Behaviour of Composite Structures Reinforced with Continuous Fibers *Materiale Plastice* **49**(3) 186-191.

[20]   Gillich G R, Birdeanu E D, Gillich N, Amariei D, Iancu V and Jurca C S 2009 Detection of damages in simple elements *Annals of DAAAM for 2009 & Proceedings of the 20th International DAAAM Symposium* **20** 623-624.

[21]   Onchis-Moaca D, Gillich G R and Frunza R 2012 Gradually Improving The Readability Of The Time-Frequency Spectra For Natural Frequency Identification In Cantilever Beams 2012 Proceedings of the 20th European Signal Processing Conference (EUSIPCO) 809-813.

[22]   Gillich G R, Maia N M M, Mituletu I C, Praisach Z I, Tufoi M and Negru I 2015 Early Structural Damage Assessment by Using an Improved Frequency Evaluation Algorithm *Latin American Journal of Solids and Structures* **12**(12) 2311-2329.

[23]   Cawley P and Adams R D 1979 The locations of defects in structures from measurements of natural frequencies *Journal of Strain Analysis* **14**(2) 49–57.

[24]   Gillich G R, Abdel Wahab M, Praisach Z I and Ntakpe J L 2014 The influence of transversal crack geometry on the frequency changes of beams *Proceedings of International Conference on Noise and Vibration Engineering (ISMA2014) and International Conference on Uncertainty in Structural Dynamics (USD2014)* 485-498.